ZnCdO/ZnO Coaxial Multiple Quantum Well Nanowire Heterostructures and Optical Properties

Chuanwei Cheng,[†] Bo Liu,[†] Edbert Jarvis Sie,[†] Weiwei Zhou,[†] Jixuan Zhang,[‡] Hao Gong,[‡] Cheng Hon Alfred Huan,[†] Tze Chien Sum,*[,†] Handong Sun,[†] and Hong Jin Fan*[,†]

Division of Physics and Applied Physics, School of Physical and Mathematical Sciences, Nanyang Technological University, Singapore 637371, Singapore, and Department of Materials Science and Engineering, National University of Singapore, 117576, Singapore

Received: November 29, 2009; Revised Manuscript Received: January 20, 2010

High quality vertical-aligned arrays of ZnCdO/ZnO coaxial multiple-quantum-well (MQW) nanowire heterostructures are fabricated for the first time by combining a simple chemical vapor deposition (CVD) and pulsed laser deposition (PLD) method. The ZnO nanowire core enables epitaxial and dislocation-free growth of uniform ZnCdO/ZnO quantum wells. Both steady-state and time-resolved photoluminescence measurements of the MQW nanowires are performed in the temperature range of 10−300 K. Strong quantum confinement and carrier localization effect are verified. In addition, an S-shaped temperature dependence is observed for both the exciton emission energy (E_p) and their lifetime in ZnCdO MQWs, which has not previously been reported in ZnMgO MQWs. A simple phenomenological model was introduced to explain this anomalous behavior. Such ZnCdO/ZnO coaxial MQW nanowires might find applications in nanoscale laser sources and other oxide-based quantum devices.

Introduction

Rational design and synthesis of complex and multicomponent one-dimensional structures can yield enhanced and/or novel electronic and photonic functions.[1−7] Among direct band gap materials, ZnO with wide band gap (∼3.37 eV) and large exciton binding energy (60 meV) at room temperature has been a promising candidate for many applications such as ultraviolet lasers,[8] solar cells,[9] sensors,[10,11] and light emitting diodes.[12] Moreover, its flexibility to tune the band gap (E_g) such that 2.3 eV < E_g < 4.0 eV by alloying[13] with Cd or Mg enables the light emission from the deep UV to the visible region. In particular, quantum well structures which provide both electrical and optical confinement are ideal candidates for optoelectronic devices.[14] Motivated by this, studies on ZnO-based quantum structures and their optical properties[13−18] have gathered great interest in the past few years. So far, the focus is ZnO/ZnMgO heteronanostructures including multiple quantum wells (MQWs). For example, the Yi group has successfully prepared ZnO/ZnMgO nanowire and nanotube heterostructures by metal−organic vapor phase epitaxy (MOVPE).[19−21] There are also a few reports on ZnCdO/ZnO thin-film quantum wells in spite of the lower solubility of Cd in ZnO.[22−26] Nevertheless, to the best of our knowledge, ZnCdO/ZnO coaxial MQW nanowires have not been reported yet. As ZnCdO has a reduced band gap compared to ZnO, the heterostructure differs from ZnO/ZnMgO that, in the former, the alloy composition lies in the quantum wells. Therefore, the ZnCdO/ZnO coaxial MQW nanowires are highly desirable not only for exploring new physical properties but also for their potential applications in nanoscale opto-electronic devices as mentioned above.

In this study, we report on the first successful fabrication of ZnCdO/ZnO coaxial MQW nanowire arrays on GaN/sapphire substrates using a relatively simple and low-cost approach by combining chemical vapor deposition (CVD) and pulsed laser deposition (PLD). The steady-state and time-resolved photoluminescence (PL) properties of these nanostructures were studied as a function of temperature, from which an anomalous S-shaped temperature dependence of both the excitons (E_p) and lifetime (τ_p) from the QWs was observed. The carrier dynamics measurement of the MQWs allows an identification of the photoinduced carrier recombination and relaxation kinetics, as well as the origin of the S-shaped behavior.

Experimental Section

Sample Preparation. ZnO nanowire arrays were grown on GaN/sapphire substrates by a simple CVD method. In a typical process: A ∼4 nm Au film was deposited on GaN/sapphire substrates by sputtering. ZnO powder (Sigma Aldrich, 99.9%) and graphite powder (Sigma Aldrich, 99%) with 3:2 weight ratio were grounded and loaded to an alumina boat. Then, the Au sputter-coated GaN/sapphire substrates and the alumina boat were placed in a small quartz tube (diameter 15 mm, length 300 mm). The substrates were typically put 4−8 cm away from the center of the boat. This quartz tube was then placed inside a furnace quartz tube, with the center of the alumina boat positioned at the center of the furnace and the substrates placed downstream of an argon flow. The temperature of the furnace was ramped to 925 °C at a rate of 50 °C/min and kept at that temperature for 3 min under a constant flow of 30 sccm Ar and a pressure of 20 mbar.The obtained ZnO nanowire arrays were subsequently transferred into a PLD chamber. MQW nanowire heterostructure arrays were fabricated by alternative depositions of ZnCdO and ZnO layers. The growth temperature and oxygen partial pressure were kept constant at 550 °C and 10 mTorr, respectively. The nanowires consist of 4 MQWs, with ∼1.5 nm

* Corresponding author. E-mail: tzechien@ntu.edu.sg (T.C.S.); fanhj@ntu.edu.sg (H.J.F.).
[†] Nanyang Technological University.
[‡] National University of Singapore.

10.1021/jp911310r
Published on Web 02/10/2010

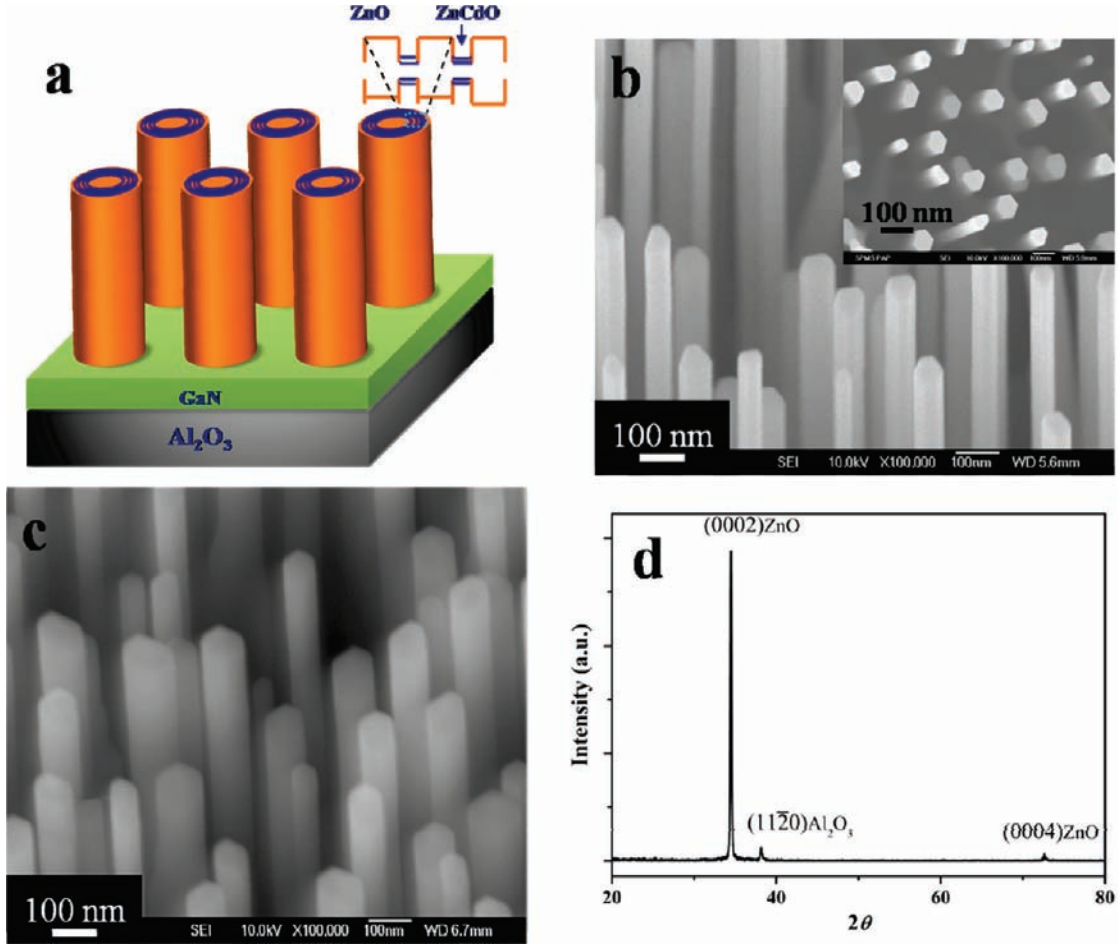

Figure 1. (a) Schematics of the structure and energy band diagram of the ZnCdO/ZnO MQWs. (b) 20° tilted SEM images of bare ZnO nanowire arrays. Inset: top view. (c) SEM image and (d) XRD pattern of the ZnCdO/ZnO MQW nanowire arrays.

thick $Zn_{0.962}Cd_{0.038}O$ wells and ~4.5 nm thick ZnO barriers, as schematically depicted in Figure 1a.

Characterization and Optical Measurements. The morphology and microstructures of the as prepared ZnO and the MQWs were examined using JEOL JSM-6700F field emission scanning electron microscopy (FE-SEM) and JEM 2010F transmission electron microscopy (TEM). The X-ray powder diffraction (XRD) pattern was recorded with a Bruker D8 Advanced diffractometer using Cu Kα as the radiation source. PL measurements were performed in the temperature range from 10 to 300 K within a closed cycle helium cryostat using the 325 nm line of a continuous-wave He−Cd laser for excitation. For the time-resolved PL measurements, the sample was excited by 325 nm laser pulses generated from an optical parametric amplifier (Coherent TOPAZ) that was pumped using a 100 fs, 1 kHz regenerative amplifier (Coherent Legend). The on-axis peak power is $I_{00} = 0.25$ mJ/cm^2. The luminescence was collected in a conventional backscattering geometry and was spectrally dispersed by a DK240 1/4 m monochromator with 300 g/mm grating, and the temporal information was measured using an Optronis Optoscope streak camera system. A fast triggered sweep unit (Optronis FTSU1-ST) with an ultimate temporal resolution of ~10 ps was used for the data collection. The streak camera and the femtosecond laser were synchronized using an electronic delay unit. The streak camera images were recorded using a 12-bit cooled CCD readout unit (Optronis SCRU-SE). The images obtained were averaged over 500 accumulated images. The PL decays were extracted over a 7 nm range about the associated emission peaks and are best fitted with monoexponential PL decays.

Results and Discussion

Figure 1 shows the schematics and SEM images of both bare ZnO nanowires and ZnCdO/ZnO MQW structures. The bare ZnO nanowires have an average diameter of 65 nm and a length of ~1 μm, and a vertical alignment due to the epitaxial growth.[27] After the PLD of MQWs, there was no significant change in morphology except that the nanowire diameters were enlarged, which is ascribed to the continuous growth of the ZnCdO (well) and ZnO (barrier) layers. The X-ray diffraction (XRD) spectrum (Figure 1d) of the MQW nanowires shows a predominant peak at 34.5° corresponding to the (0002) plane of wurtzite ZnO. The appearance of (0002) is consistent with the vertical alignment of the nanowires along the *c*-direction and normal to the substrate surface. A small diffraction peak from the a-plane alumina substrate is also observed.

The single crystalline ZnO nanowire cores enable an epitaxial and dislocation-free growth of highly uniform (ZnCdO/ZnO) quantum wells. TEM images (Figure 2a) show that the core−shell structures are smooth both in their surface and interface. The total thickness of the multishell layers is about 22 nm. High-resolution TEM images and electron diffraction patterns (Figure 2b and c) reveal that the total nanowire is single crystalline without interfacial defects. Because of the small percentage (3.8%) of Cd, the lattice structure is nearly unchanged; thus, the diffraction pattern of the ZnCdO/ZnO MQW nanowire is similar to the pristine ZnO nanowire. On the basis of the fabrication, there are four layers of ZnCdO, each with a nominal thickness of 1.5−2 nm.

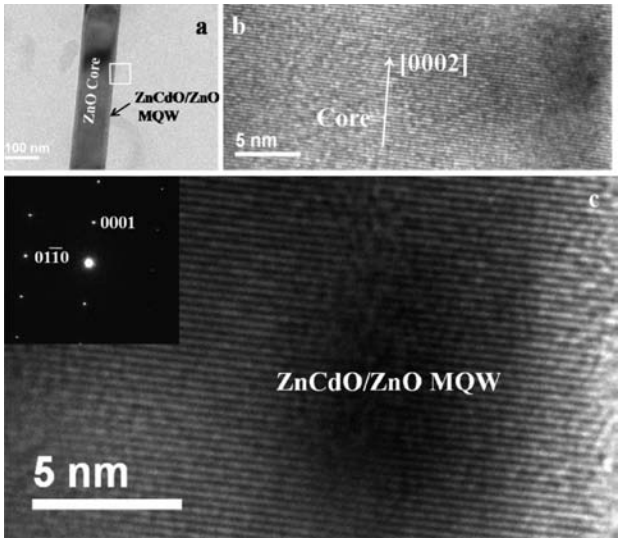

Figure 2. (a) TEM image of the ZnCdO/ZnO nanowire MQW. (b) High resolution TEM image taken from (b) the ZnO nanowire core and (c) the MQW shell. Inset: corresponding selected area electron diffraction pattern (SAED) recorded from the shell region.

The optical properties of the MQW nanowire heterostructures were characterized using PL spectroscopy. Figure 3a shows the 10 K PL spectra of the pristine ZnO nanowires. The dominant peaks at 3.354 and 3.358 eV are ascribed to the neutral donor-bound exciton (D^0X) in ZnO nanowires.[28] The A-free exciton emission (FX_A) at 3.369 eV is also observed. At a lower energy side of D^0X, the peak at 3.306 eV is ascribed to the longitudinal optical (LO) phonon of FX_A. Here, the energy separation of 63 meV between FX_A-LO and FX_A is smaller than the LO phonon energy (72 meV), which is due to the energy softening of FX_A-LO.[29] The other lower-energy peaks resolved at 3.236, 3.166, 3.095, 3.023, and 2.950 eV are from the donor−acceptor pair (DAP) as well as its four-order LO-phonon replicas with a constant energy separation of 70−73 meV.[30] For the ZnCdO/ZnO MQW nanowires, a new peak centered at 3.2 eV dominates the PL spectrum, as shown in Figure 3a. As this peak is not present in the bare ZnO nanowires, it is believed to be the ZnCdO QW-related emission due to an evident quantum confinement effect (see below for other evidence). Thus, it shows that Cd has been successfully incorporated in the coaxial MQW nanowires.

For comparison, ZnCdO/ZnO coaxial nanowires with a ∼15 nm thick single shell of ZnCdO (i.e., same composition but no QW structure) were also prepared under the same conditions (see Figure S1 of the Supporting Information). The corresponding 10 K PL spectrum (Figure 3b) show a predominant peak centered at 3.354 eV from the ZnO core, and a small broad feature centered at ∼3.11 eV which is emitted from the ZnCdO alloy layer. The energy position for $Zn_{0.962}Cd_{0.038}O$ can be estimated on the basis of the equation $E_{PL} = 3.37 - 12.4x + 92.28x^2$ (eV) in ref 31 to be 3.02 eV. Note that, compared with the QW-related emission in Figure 3a, the peak from this ZnCdO alloy layer has a much smaller intensity and lower energy due to the absence of the quantum confinement effect.

To quantitatively check the strength of quantum confinement in our samples, the lowest energy level within the QW is estimated on the basis of the transcendental equation by assuming a 1-D square quantum well structure (see the Supporting Information). The calculation results in $\Delta E = 0.11$ eV, which is in agreement with our experimental data that the PL peak from the MQW is ∼0.11 eV higher than that from the

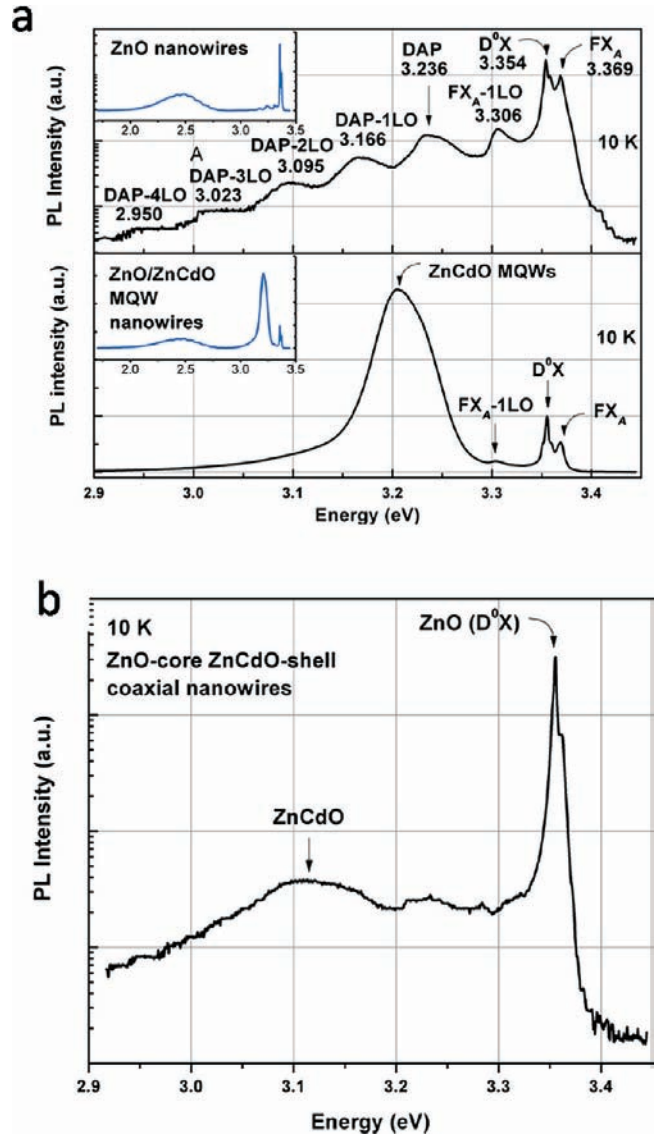

Figure 3. (a) 10 K PL spectra of bare ZnO nanowire arrays and ZnO/ZnCdO MQW nanowire arrays. (b) 10 K PL spectra of ZnCdO/ZnO coaxial nanowires. The nanowire has a single outer layer of $Zn_{0.932}Cd_{0.038}O$.

ZnCdO core−shell structures. Hence, we believe there exists a strong quantum confinement within our sample.

To further investigate the effect of exciton localization in the MQWs, temperature-dependent PL spectra were collected. The normalized PL spectra measured from 10 to 300 K are presented in Figure 4. The intensity of the ZnCdO QW-related emission and near band gap emission of ZnO decrease with increasing temperature, which is partly due to the increased nonradiative recombination. Also clear is that the relative intensity of FX_A increases, whereas that of D^0X decreases and becomes undetectable at temperatures above 80 K. Note that the FX_A-1LO emission can be traced up to ∼230 K. Interestingly, the QW-related PL emission shows a different energy shift behavior with increasing temperature compared with those of FX_A, D^0X, and FX_A-1LO: the former exhibits an S-shaped trend. For closer inspection, the temperature dependences of all PL peaks are plotted in Figure 5a. As seen in this figure, the FX_A, FX_A-LO, and D^0X peak energies show a monotonic redshift with increasing temperature. It is well established that the temperature-induced fundamental gap shrinkage of ZnO can be described by the Varshni empirical equation due to electron−lattice

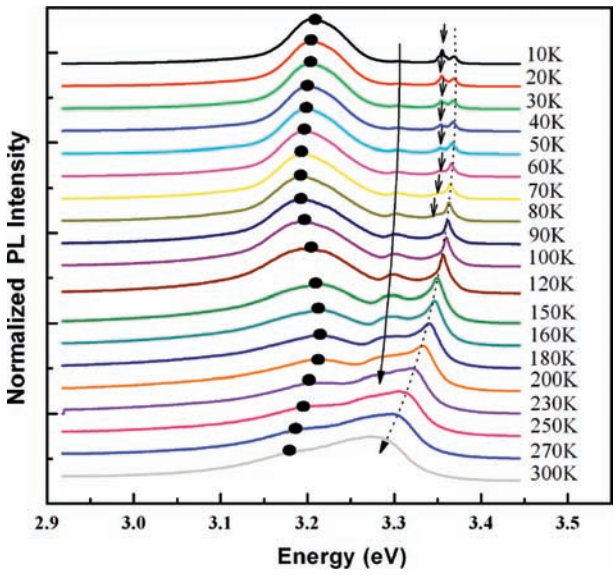

Figure 4. Temperature dependent PL spectra of the nanowire MQWs in the range from 10 to 300 K. Solid circles show the evolution of the QW related emission. The dashed line indicates the peak evolution of the FX_A emission, and the solid line shows the trend of FX_A-1LO. The arrows denote the D^0X peak. All of the spectra are normalized and shifted in the vertical direction for clarity.

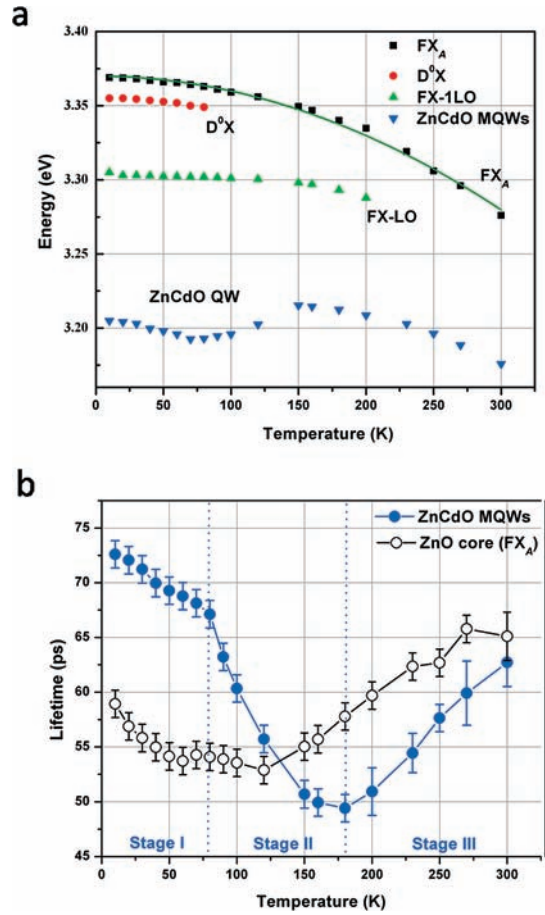

Figure 5. (a) PL peak energies plotted as a function of temperature. The solid line curves represent the best fit according to the Varshni equation. (b) Time-resolved PL results of the PL decay from the ZnCdO/ZnO coaxial MQW nanowire sample in the temperature range 10−300 K. Solid and empty circles correspond to the PL decay of the QW-related peak and the FX_A peak. The error bars are taken by considering the standard deviation of repeated time-resolved PL measurements and the intrinsic temporal resolution of the instrument.

interaction,[32] $E_g(T) = E_g(0) - \alpha T^2/(\beta + T)$, where $E_g(0)$ is the band gap at 0 K and α and β are Varshni thermal coefficients. The temperature dependent PL peak for the FX_A emission of ZnO is consistent with the estimated energy decrease of about 93 meV at 300 K. However, the ZnCdO QW-related PL emission does not follow the conventional trend at temperatures of ∼120 K due to the carrier localization effect. Instead, it exhibits an anomalous S-shaped temperature dependence of the peak energy (E_p). As the temperature increases from 10 to 80 K, E_p redshifts by 12 meV, which then blueshifts by 22 meV in the temperature range 80−180 K. When the temperature is further increased above 180 K, the peak redshifts again. A similar S-shaped behavior has also been observed previously in the InGaN[33] and AlGaN[34] QW systems, as well as very recently in the ∼10 nm thick ZnCdO alloy films,[35] which is ascribed to the potential fluctuation, as a consequence of the inhomogeneous alloy composition and/or roughness interface. For comparison, the temperature dependent PL spectra of the ZnCdO/ZnO core−shell nanowire sample were measured, and a slight S-shaped behavior was also observed in the ZnCdO alloy related emission peak (Figure S2 of the Supporting Information). It has been previously reported that the degree of carrier localization is strongly correlated with the composition concentrations, well width, and interface roughness.[36,37] In our case, we think the MQW sample may provide much stronger carrier localization confinement than that of the core−shell heterostructure sample, leading to the difference in PL spectra. The origin of the anomalous temperature dependence of E_p in our ZnCdO/ZnO MQWs will be discussed later.

Temperature-dependent time-resolved PL measurements were performed to elucidate the carrier dynamics in these MQWs. Figure 5b shows a comparison of the PL lifetimes originating from the confined carriers in MQWs and that of the free excitons (FX_A) from the ZnO nanowire core of the same sample. All of the peak decays were fitted by using a monoexponential decaying function: $I(t) = Ae^{-t/\tau}$, where τ is the PL lifetime and A is the normalization constant. As seen from Figure 5b, the carrier dynamics in the MQWs exhibits distinct behavior in three temperature ranges: stage I (10−80 K), relatively longer lifetime at ∼70 ps that gradually decreases with increasing temperature; stage II (80−180 K), a more rapid transition of dynamics from ∼65 to ∼50 ps; stage III (180−300 K), gradual transition of dynamics from ∼50 ps back to ∼65 ps. In contrast, the FX_A dynamics of the core ZnO exhibits rather different behavior, i.e., the absence of stage II. Interestingly, by comparing Figure 5a and b, one can see that the temperature range for the S-shaped energy shift coincides with that of the recombination lifetime. This suggests that the carrier dynamics are strongly related to a variation of energy levels within the QWs.

On the basis of the above results, a phenomenological recombination mechanism in ZnCdO QWs can be proposed: The intrinsic unit cell of bulk CdO crystal (4.69 Å) is known to be slightly larger than bulk ZnO crystal (4.47 Å). The Cd dopant replaces the Zn in the ZnO lattice. This introduces a lattice expansion in the immediate vicinity of the Cd site and induces a local potential perturbation. As the Cd dopants are randomly distributed in the host crystal, the variation of local interaction depends on the local density of Cd atoms. This brings about a spatial potential fluctuation or the band tailing effect on the total density of states. In addition, the intrinsic electric field arising from the spontaneous polarization difference at the ZnCdO/ZnO interface could possibly introduce a Frank−Keldysh

effect. However, the later effect can be ignored as the Cd and Zn have a negligible difference in their electronegativity within this sample. Hence, the differences between the trend in the temperature dependence of the recombination lifetimes ($\tau_{PL}^{-1} = \tau_{Radiative}^{-1} + \tau_{Nonradiative}^{-1}$) for MQWs and the ZnO core (FX_A emission) can be mainly attributed to the potential fluctuation.

We describe the anomalous temperature dependence of the carrier dynamics in the MQWs as follows: Upon photoexcitation, at low temperatures (10−80 K), the carriers are rapidly captured by the local potential dips within the MQWs. The thermal energy is insufficient to promote the carriers to the laterally delocalized states. Hence, the wave function overlap between the electron and hole is weak, resulting in smaller recombination efficiency (i.e., longer lifetimes). Both the carrier dynamics and the energy shift follow the trend of the ZnO core (FX_A) in this region. In addition, it is likely that, as the temperature increases from 10 to 80 K, more acoustic phonons are activated. The presence of defects and the increased carrier−phonon scattering results in the increased contribution from the nonradiative pathways. This is evident in the decreased PL recombination lifetimes for both the MQWs and ZnO core. As the temperature is increased further (80−180 K), the carriers gain sufficient thermal energy to be delocalized to higher energy states within the MQW. Due to the stronger wave function overlap compared to the earlier scenario, the carriers undergo radiative recombination more effectively. This increase in oscillator strength results in shorter recombination lifetimes, as evidenced by the rapid drop of PL lifetime (Figure 5b). The increased probability for carriers to be excited to higher energy states (arising from the local potential fluctuation) brings about the broadening to the high energy side of the emission spectrum, resulting in a blueshift in the peak energy (see Figure 5a). At sufficiently high temperatures above 180 K, the potential fluctuations are screened by the thermal agitations and the carrier dynamics follow a trend similar to that of the ZnO core. Hence, the peak position exhibits a redshift again. The carrier dynamics in this stage can be explained as follows. Feldmann et al.[38] previously established that there is a linear correlation between the spectral line width and the radiative exciton lifetimes in quantum wells (i.e., broader linewidth corresponds to longer lifetimes). We believe that a similar relationship is observed in our samples at stage III (above 180 K) where the carriers in the QWs are thermally delocalized (as well as those in the ZnO core prior to this stage). The observed radiative transitions arise from the sharing of the $k = 0$ oscillator strength equally among all states within the finite spectral width, $\Delta(T)$. Due to increased carrier−phonon interactions which redistribute the carrier populations, the excitons away from $k = 0$ (within the spectral width $\Delta(T)$ in k-space) also contribute to the radiative transitions. Hence, the carrier dynamics at this stage in the QWs and the ZnO core are similar.

Conclusions

In summary, for the first time, we have successfully fabricated ZnO/ZnCdO coaxial MQW nanowire heterostructures by combining a simple CVD and PLD method. PL investigations have demonstrated that such MQWs exhibit a strong quantum confinement effect. An S-shaped temperature dependence of the exciton emission peak energy (E_p) from the ZnCdO QW is observed, which is proposed to be related to spatial potential fluctuations caused by the inhomogeneous Cd distribution. In addition, time-resolved PL spectroscopy reveals that the confined-carrier dynamics in the MQWs exhibit distinct behavior in comparison with the FX_A dynamics of the core ZnO. A phenomenological model is proposed to explain this anomalous behavior. Such ZnCdO/ZnO coaxial MQW nanowire heterostructures might find applications in nanoscale laser sources and other oxide-based quantum devices.

Acknowledgment. This work is supported by the start-up funding from Nanyang Technological University to H.J.F. (Grant No. M58110048) and T.C.S. (Grant No. M58110068).

Supporting Information Available: SEM image and TEM image of ZnCdO/ZnO coaxial nanowires, temperature-dependent PL spectra of the ZnCdO/ZnO coaxial nanowires, and calculation of the peak energy of QW. This material is available free of charge via the Internet at http://pubs.acs.org.

References and Notes

(1) Agarwal, R. *Small* **2008**, *4*, 1872–1893.
(2) Mieszawska, A. J.; Jalilian, R.; Sumanasekera, G. U.; Zamborini, F. P. *Small* **2007**, *3*, 722–756.
(3) Fan, H. J.; Yang, Y.; Zacharias, M. *J. Mater. Chem.* **2009**, *19*, 885–900.
(4) Xiang, J.; Vidan, A. R.; Westervelt, M.; Lieber, C. M. *Nat. Nanotechnol.* **2006**, *1*, 208–213.
(5) Qian, F.; Li, Y.; Gradecak, S.; Park, H.-G.; Dong, Y. J.; Ding, Y.; Wang, Z. L.; Lieber, C. M. *Nat. Mater.* **2008**, *7*, 701–706.
(6) Hua, B.; Motohisa, J.; Kobayashi, Y.; Hara, S.; Fukui, T. *Nano Lett.* **2009**, *9*, 112–116.
(7) Cheng, C. W.; Liu, B.; Yang, H. Y.; Zhou, W. W.; Sun, L.; Chen, R.; Yu, S. F.; Zhang, J. X.; Gong, H.; Sun, H. D.; Fan, H. J. *ACS Nano* **2009**, *3*, 3069–3076.
(8) Huang, M. H.; Mao, S.; Feick, H.; Yan, H. Q.; Wu, Y. Y.; Kind, H.; Weber, E.; Russo, R.; Yang, P. D. *Science* **2001**, *292*, 1897–1899.
(9) Lorie, M.; Johnson, G. J.; Saykally, R.; Yang, P. D. *Nat. Mater.* **2005**, *4*, 455–459.
(10) Cheng, C. W.; Xu, G. Y.; Zhang, H. Q.; Luo, Y. *J. Nanosci. Nanotechnol.* **2007**, *7*, 4439–4442.
(11) Cheng, C. W.; Xu, G. Y.; Zhang, H. Q.; Luo, Y.; Zhang, P. G.; Shen, K. *Mater. Res. Bull.* **2008**, *43*, 3506–3513.
(12) Lim, J. H.; Kang, C. K.; Kim, K. K.; Park, I. K.; Hwang, D. K.; Park, S. J. *Adv. Mater.* **2006**, *18*, 2720–2724.
(13) Makino, T.; Segawa, Y.; Kawasaki, M.; Ohtomo, A.; Shiroki, R.; Tamura, K.; Yasuda, T.; Koinuma, H. *Appl. Phys. Lett.* **2001**, *78*, 1237–1239.
(14) Koike, K.; Hama, K.; Nakashima, I.; Takada, G. Y.; Ozaki, M.; Qgata, K. I.; Sasa, S. M.; Inoue, M.; Yano, M. *Jpn. J. Appl. Phys.* **2004**, *43*, L1372−1375.
(15) Fan, Z. Y.; Chang, P. C.; Lu, J. G.; Walter, E. C.; Penner, R. M.; Lin, C. H.; Lee, H. P. *Appl. Phys. Lett.* **2004**, *85*, 6128–6130.
(16) Djurisic, A. B.; Leung, Y. H. *Small* **2006**, *2*, 944–961.
(17) Klingshirn, C. *Phys. Status Solidi B* **2007**, *244*, 3027–3073.
(18) Willander, M.; Nur, O.; Zhao, Q. X.; Yang, L. L.; Lorenz, M.; Cao, B. Q.; Pérez, J. Z.; Zekalla, C. C.; Zimmermann, G.; Grundmann, M.; Bakin, A.; Behrends, A.; AlSuleiman, M.; El-Shaer, A.; Mofor, A. C.; Postels, B.; Waag, A.; Boukos, N.; Travlos, A.; Kwack, H. S.; Guinard, J.; Dang, D. L. S. *Nanotechnology* **2009**, *20*, 332001–332040.
(19) Park, W. I.; Yi, G.-C.; Kim, M.; Pennycook, S. J. *Adv. Mater.* **2003**, *15*, 526–528.
(20) Jang, E.-S.; Bae, J. Y.; Yoo, J.; Park, W. I.; Kim, D.-W.; Yi, G.-C.; Yatsui, T.; Ohtsu, M. *Appl. Phys. Lett.* **2006**, *88*, 023102−023104.
(21) Yoo, J. Y.; Hong, Y. J.; Jung, H. S.; Kim, Y.-J.; Lee, C.-H.; Cho, J. H.; Doh, Y.-J.; Dang, L. S.; Park, K. H.; Yi, G.-C. *Adv. Funct. Mater.* **2009**, *19*, 1601–1608.
(22) Kalusniak, S.; Sadofev, S.; Puls, J.; Henneberger, F. *Laser Photonics Rev.* **2009**, *3*, 233–242.
(23) Sadofev, S.; Kalusniak, S.; Puls, J.; Schäfer, P.; Blumstengel, S.; Henneberger, F. *Appl. Phys. Lett.* **2007**, *91*, 231103–231105.
(24) Thompson, A. V.; Boutwell, C.; Mares, J. W.; Schoenfeld, W. V.; Osinsky, A.; Hertog, B.; Xie, J. Q.; Pearton, S. J.; Norton, D. P. *Appl. Phys. Lett.* **2007**, *91*, 201921–201923.
(25) Lim, W.; Norton, D. P.; Pearton, S. J.; Wang, X. J.; Chen, W. M.; Buyanova, I. A.; Osinsky, A.; Dong, J. W.; Hertog, B.; Thompson, A. V.; Schoenfeld, W. V.; Wang, Y. L.; Ren, F. *Appl. Phys. Lett.* **2008**, *92*, 032103−032105.
(26) Buyanova, I. A.; Wang, X. J.; Pozina, G.; Chen, W. M.; Lim, W.; Norton, D. P.; Pearton, S. J.; Osinsky, A.; Dong, J. W.; Hertog, B. *Appl. Phys. Lett.* **2008**, *92*, 261912–26194.

(27) Fan, H. J.; Fuhrmann, B.; Scholz, R.; Himcinschi, C.; Berger, A.; Leipner, H.; Dadgar, A.; Krost, A.; Christiansen, S.; Gösele, U.; Zacharias, M. V. *Nanotechnology* **2006**, *17*, S231–S239.

(28) Teke, A.; Özgür, Ü.; Dogan, S.; Gu, X.; Morkoç, H.; Nemeth, B.; Nause, J.; Everitt, H. O. *Phys. Rev. B* **2004**, *70*, 195207-1-10.

(29) Meng, X. Q.; Shen, D. Z.; Zhang, J. Y.; Zhao, D. X.; Dong, L.; Lu, Y. M.; Liu, Y. C.; Fan, X. W. *Nanotechnology* **2005**, *16*, 609–612.

(30) Meyer, B. K.; Alves, H. D.; Hofmann, M.; Kriegseis, W.; Forster, D.; Bertram, F.; Christen, J.; Hoffmann, A.; Straβburg, M.; Dworzak, M.; Haboeck, U.; Rodina, A. V. *Phys. Status Solidi B* **2004**, *241*, 231–259.

(31) Kang, H. S.; Kim, J. W.; Kim, J. H.; Lee, S. Y.; Li, Y.; Lee, J. S.; Lee, J. K.; Nastasi, M. A.; Crooker, S. A.; Jia, Q. X. *J. Appl. Phys.* **2004**, *99*, 066113−066115.

(32) Varshni, Y. P. *Physica* **1967**, *34*, 149–154.

(33) Cho, Y -H.; Gainer, G. H.; Fischer, A. J.; Song, J. J.; Keller, S.; Mishra, U. K.; DenBaars, S. P. *Appl. Phys. Lett.* **1998**, *73*, 1370–1372.

(34) Bell, A.; Srinivasan, S.; Plumlee, C.; Omiya, H.; Phonce, F. A.; Tanaka, J. S.; Fujioka, A.; Nakagawa, Y. *J. Appl. Phys.* **2004**, *95*, 4670–4674.

(35) Lange, M.; Zippel, J.; Benndorf, G.; Czekalla, C.; Kochmuth, H.; Lorenz, M.; Grundamann, M. *J. Vac. Sci. Technol., B* **2009**, *27*, 1741–1745.

(36) Shu, G. W.; Shu, Wu. P.; Wu, F.; Lo, M. H.; Shen, J. L.; Lin, T. Y.; Chang, H. G.; Chen, Y. F.; Shif, C. F.; Chang, C. A.; Chen, N. C. *Appl. Phys. Lett.* **2006**, *89*, 131913–131915.

(37) Na, J. H.; Taylor, R. A.; Lee, K. H.; Wang, T.; Tahraoui, A.; Parbrook, P.; Fox, A. M.; Yi, S. N.; Park, Y. S.; Choi, J. W.; Lee, J. S. *Appl. Phys. Lett.* **2006**, *89*, 253120–253122.

(38) Feldmann, J.; Peter, G.; Göbel, E. O.; Dawson, P.; Moore, K.; Foxon, C.; Elliott, R. J. *Phys. Rev. Lett.* **1987**, *59*, 2337–2340.

JP911310R